



RESEARCH LETTER

10.1002/2016GL072305

Key Points:

- First decade-long ammonia records (2002–2016) were retrieved from AIRS satellite daily measurements
- Substantial increases in ammonia concentrations are observed over several of the world's major agricultural regions
- Causes of ammonia increase include increased fertilizer use, increasing temperatures, and decreased loss to aerosols

Correspondence to:

J. X. Warner,
 juying@atmos.umd.edu

Citation:

Warner, J. X., R. R. Dickerson, Z. Wei, L. L. Strow, Y. Wang, and Q. Liang (2017), Increased atmospheric ammonia over the world's major agricultural areas detected from space, *Geophys. Res. Lett.*, 44, doi:10.1002/2016GL072305.

Received 9 DEC 2016
 Accepted 18 FEB 2017

Increased atmospheric ammonia over the world's major agricultural areas detected from space

J. X. Warner¹ , R. R. Dickerson¹ , Z. Wei¹ , L. L. Strow² , Y. Wang³, and Q. Liang^{4,5}

¹Department of Atmospheric and Oceanic Science, University of Maryland, College Park, Maryland, USA, ²Department of Physics and Joint Center for Environmental Technology, University of Maryland, Baltimore County, Baltimore, Maryland, USA, ³Department of Earth and Atmospheric Sciences, University of Houston, Houston, Texas, USA, ⁴Atmospheric Chemistry and Dynamics, NASA Goddard Space Flight Center, Greenbelt, Maryland, USA, ⁵Universities Space Research Association-GESTAR, Columbia, Maryland, USA

Abstract This study provides evidence of substantial increases in atmospheric ammonia (NH₃) concentrations (14 year) over several of the world's major agricultural regions, using recently available retrievals from the Atmospheric Infrared Sounder (AIRS) aboard NASA's Aqua satellite. The main sources of atmospheric NH₃ are farming and animal husbandry involving reactive nitrogen ultimately derived from fertilizer use; rates of emission are also sensitive to climate change. Significant increasing trends are seen over the U.S. (2.61% yr⁻¹), the European Union (EU) (1.83% yr⁻¹), and China (2.27% yr⁻¹). Over the EU, the trend results from decreased scavenging by acid aerosols. Over the U.S., the increase results from a combination of decreased chemical loss and increased soil temperatures. Over China, decreased chemical loss, increasing temperatures, and increased fertilizer use all play a role. Over South Asia, increased NH₃ emissions are masked by increased SO₂ and NO_x emissions, leading to increased aerosol loading and adverse health effects.

1. Introduction

Atmospheric ammonia (NH₃) is an important component of the global nitrogen cycle [Galloway and Cowling, 2002; Galloway et al., 2008; Sutton et al., 2007, 2008; Erismann et al., 2008, 2013; Fowler et al., 2013, 2015]. In the troposphere ammonia reacts rapidly with acids such as sulfuric (H₂SO₄), nitric (HNO₃) to form fine particulate matter (PM_{2.5}) [Malm et al., 2004]. These ammonium (NH₄⁺) containing aerosols affect Earth's radiative balance, both directly by scattering incoming radiation [Adams et al., 2001; Martin et al., 2004; Henze et al., 2012] and indirectly as cloud condensation nuclei [Abbatt et al., 2006]. PM_{2.5} endangers public health by penetrating the human respiratory systems, depositing in the lungs and alveolar regions [Pope et al., 2002], and causing premature mortality [Lelieveld et al., 2015]. A precursor of these inorganic aerosols, gaseous NH₃ is often the limiting species in their formation [Wang et al., 2013; Lelieveld et al., 2015]. Excess reactive nitrogen reduces biodiversity and causes harmful algal blooms and anoxic conditions. Dry deposition of gaseous ammonia may have substantially greater adverse impacts on ecosystem health than deposition of ammonium in aerosols or precipitation [Sheppard et al., 2011]. In contrast, PM_{2.5} has greater impact on human morbidity and mortality. In this article we quantify recent (~14 year) increases in tropospheric ammonia and suggest likely causes for these trends.

Major sources of atmospheric ammonia involve agricultural activities including animal husbandry, especially concentrated animal feeding operation, and fertilizer use [Streets et al., 2003; Huang et al., 2012; Hauglustaine et al., 2014; Riddick et al., 2016]. Ammonium fertilizers are essential in high-yield crop production and contribute substantially atmospheric NH₃. Fertilizer usage in China (~31.2 Tg N yr⁻¹ and ~+2.7% yr⁻¹) and India (~18.8 Tg N yr⁻¹ and ~+3.6% yr⁻¹) has increase several fold in the last two decades, from Earth Policy Institute (http://www.earth-policy.org/data_highlights/2014/highlights43) and according to the World Bank (<http://data.worldbank.org/indicator/AG.CON.FERT.ZS>). It is estimated that 50% of the total NH₃ emission in 2000 in China came from fertilizer application and another 38% from other agricultural sources [Streets et al., 2003]. Ammonia emissions increase with increasing nitrogen content and pH of soils and manure storage facilities, and increase exponentially with temperature (emissions roughly double between 300 and 306°K), except below freezing when emissions are near zero [Riddick et al., 2016]. A minimum level of soil moisture is also required for the microbial activities, such as urea hydrolysis, that generate NH₃. Biomass burning, highly episodic in nature, accounts for <10% of the global total but can be a locally important source [Dentener and Crutzen, 1994; Barnes and Rudzinski, 2006; Galloway et al., 2004].

Major sinks of atmospheric ammonia involve dry deposition and wet removal by precipitation, as well as conversion to particulate ammonium by reaction with acids. These acids arise primarily from the oxidation of pollutants SO_2 and NO_x ($\text{NO} + \text{NO}_2$) generated in the combustion of fossil fuels. Ammonium sulfate is generally removed by precipitation. Condensed ammonium nitrate (NH_4NO_3) exists in equilibrium with NH_3 and gas-phase HNO_3 . Lower temperatures favor the aerosol phase.

Measurements of ambient NH_3 are sparse, but satellites provide a means to monitor atmospheric composition globally. Through recent improvements in retrieval algorithms, the Atmospheric Infrared Sounder (AIRS) aboard NASA's Aqua satellite now provides daily global measurement of atmospheric NH_3 . Warner *et al.* [2016] described global NH_3 concentrations using the averaged 13 year satellite data record (2003–2015) from AIRS and provided a global perspective on its emissions, distributions, and spatial variability. They also discussed the retrieval algorithm, preliminary validation, and qualitative comparisons to measurements from other sensors. In this study, we focus on the NH_3 temporal variability, or trends, from September 2002 to August 2016 and discuss possible mechanisms underlying these trends. These AIRS NH_3 retrievals have greater daily coverages and a longer record than those from the Tropospheric Emission Spectrometer [Beer *et al.*, 2008]; and are based on higher channel sensitivities, due to the afternoon overpasses, than the Infrared Atmospheric Sounding Interferometer (IASI) [Clarisse *et al.*, 2009]. Van Damme *et al.* [2015] showed 6 year time series of NH_3 total column values over six regions of the world from IASI's early morning (9:30 A.M. local time overpass) and evening (9:30 P.M. local time overpass) measurements. Whereas they identified the relatively large emission peaks in the time series as resulting from biomass burning events, their study did not indicate clear increasing or decreasing trends. Schiferl *et al.* [2016] used a combination of observations (including IASI) and a model to evaluate variability in NH_3 over the U.S. and concluded that variability in meteorology and reduced SO_2 and NO_x emissions drive NH_3 changes observed between 2008 and 2012.

In section 2, we describe the methods and data used in the analyses, and in section 3, we present global ammonia trends. In section 4, we focus on the ammonia trends in the primary regions of interest and discuss the driving mechanisms.

2. Methods and Data

2.1. AIRS NH_3 VMRs

Warner *et al.* [2016] discussed in detail the AIRS NH_3 retrieval method, quality assurance, global NH_3 distributions, and preliminary validation. We applied additional thresholds for the trend computations. We used only NH_3 data with degrees of freedom for signal greater than 0.1, in addition to other retrieval quality assurance flags (e.g., χ^2 , retrieval residual, and cloud-cleared-radiance quality flags). All retrieval results were screened by a minimum thermal contrast determined by AIRS L2 products. If the lower layers of the atmosphere and Earth's surface have similar temperatures (low thermal contrast), they emit similar amounts of thermal radiation [Deeter *et al.*, 2007], and AIRS cannot quantify NH_3 in these layers. While AIRS NH_3 products are outputted at multiple levels from 500 hPa to the surface, here we use NH_3 VMRs at 918 hPa, where the peak sensitivity is, for this study.

For the seasonal cycles, we used a 7 day average for each region and applied an n point smoothing [Garcia, 2010]. We averaged the seasonal cycles into three periods: from 2002 to 2008, from 2009 to 2013, and from 2014 to 2016, with the mean and the 1σ standard deviations. Since we only included NH_3 concentrations from frequent sources with elevated NH_3 VMRs, the values shown in all figures maybe higher than the average concentrations in a region.

2.2. Meteorological Data Sources

As meteorological conditions influence the rate of ammonia emission and deposition, we examine surface skin temperature and total precipitation anomalies using European Centre for Medium-Range Weather Forecasts (ECMWF) ERA-Interim reanalysis (EI) [Berrisford *et al.*, 2011; Dee *et al.*, 2011]. The precipitation anomalies were computed using the 12 h forecast accumulated in each month for each ECMWF grid ($0.75^\circ \times 0.75^\circ$). Only grids containing AIRS NH_3 retrievals were considered.

For surface skin temperatures anomalies and trends, we selected ECMWF EI daytime data to match the NH_3 daytime product by only using the model outputs between 9 A.M. and 3 P.M. local times. Skin temperature

trends were based on daily means and only included the cases with NH₃ retrievals. Additionally, to avoid partial year trends, we use only skin temperatures for the period from March to August when it is sufficiently high to be most relevant to the Northern Hemisphere NH₃ emissions. The linear fits of surface skin temperatures, however, are not statistically significant as indicated by high p values; they are discussed as references only. We used the published ammonia temperature dependence [Dentener and Crutzen, 1994; Galloway et al., 2004; Riddick et al., 2016], with the expression: $E_2/E_1 = \{\exp[-10,380(1/T_2 - 1/T_1)] - 1\} * 100\%$, where T_1 is assumed to be 300 K, T_2 is T_1 plus the observed annual temperature increase, and E_1 and E_2 are NH₃ volume mixing ratios corresponding to T_1 and T_2 .

2.3. Thermal Contrasts

Remote sensing measurement sensitivities depend on surface thermal contrasts of the target areas, and in the case of NH₃, higher thermal contrast generally results in higher retrieved NH₃ concentrations. Surface thermal contrasts are defined as the differences between surface skin temperatures and surface air temperatures; however, we approximate the ECMWF 2 m air temperatures as surface air temperatures. While sufficient thermal contrast is needed for good signal-to-noise ratio, the influence of thermal contrast on the retrieved NH₃ concentrations and variability needs to be addressed, especially in trend related studies. When we examine retrievals using separate ranges of thermal contrasts in 2°K degree increments, we found that although the rates of increase/decrease in NH₃ are different in each thermal contrast range especially during winter season, the tendencies and the magnitudes are similar. Furthermore, the 14 year thermal contrast from ECMWF EI in the regions of our study shows slight decreases (i.e., $-0.016^\circ\text{K yr}^{-1}$ and $p = 0.002$ for the U.S. Midwest, $-0.021^\circ\text{K yr}^{-1}$ and $p = 0.000$ for the EU, $-0.011^\circ\text{K yr}^{-1}$ and $p = 0.053$ for China, and $-0.069^\circ\text{K yr}^{-1}$, $p = 0.000$ for South Asia). This indicates that the increasing trends of the NH₃ concentrations are not the results of the thermal contrast increasing, since the thermal contrast has decreased. We used thermal contrast daily means in March to August for trend computations and only included regions where there are NH₃ pixels.

2.4. Ozone Monitoring Instrument SO₂ and NO₂

We examine ammonia trends jointly with SO₂ and NO₂ changes to determine the scavenging by acid aerosols. We used Ozone Monitoring Instrument (OMI) level 3 SO₂ planetary boundary layer volume column density (VCD, in Dobson unit (DU)) spanning October 2005 through August 2016 (http://disc.sci.gsfc.nasa.gov/Aura/data-holdings/OMI/omso2e_v003.shtml). Strong volcanic emissions are removed from the data set by examining the daily region-wide 99.9% of SO₂ VCDs. If the percentile is found to exceed a threshold value (U.S. 5 DU, Europe 8 DU, China 10 DU, and India 8 DU), all data from that day were excluded [Krotkov et al., 2016]. Note that there are still a few large jumps of SO₂ values associated with volcanic eruptions (e.g., in 2006 and 2008), but volcanoes with a large spatial impact tend to send SO₂ into the upper troposphere where there is little NH₃.

We used OMI cloud-screened tropospheric column NO₂ (molecules/cm²) data sets similarly to SO₂. As for meteorological variables, SO₂ and NO₂ concentrations were averaged only in the areas where NH₃ retrievals were used. For OMI SO₂, the trends are only significant at 95% confidence level over China. The OMI NO₂ trends are significant at 95% confidence level for the western U.S. and the EU. The SO₂ concentrations over the U.S. are often below OMI detection limit and, therefore, not used.

3. Observed Global Ammonia Trends

Figure 1 (top) depicts a global map of the rate of change of NH₃ volume mixing ratio (VMR) in parts-per-billion by volume (ppbv) per year computed using linear regression of daily mean values in each 1° × 1° latitude-longitude grid cell. We used daily mean values in each grid to obtain Figure 1 (top). We further smoothed the results using a two-dimensional penalized least squares method allowing fast smoothing of data in one and higher dimensions by means of the discrete cosine transform [Garcia, 2010]. In addition to the general quality assurance described in section 2, we added constraints of only including grids with at least 10% of the pixels greater than 2 ppbv and records longer than 10 years. The years and locations of the biomass burning (BB) events are determined from Moderate Resolution Imaging Spectroradiometer fire products [Giglio et al., 2010] and shown in Figure 1 (top). The main agricultural (AG) regions are determined from Friedl et al. [2010]. The years of the regular fires are not shown. The fertilizer information (i.e., annual

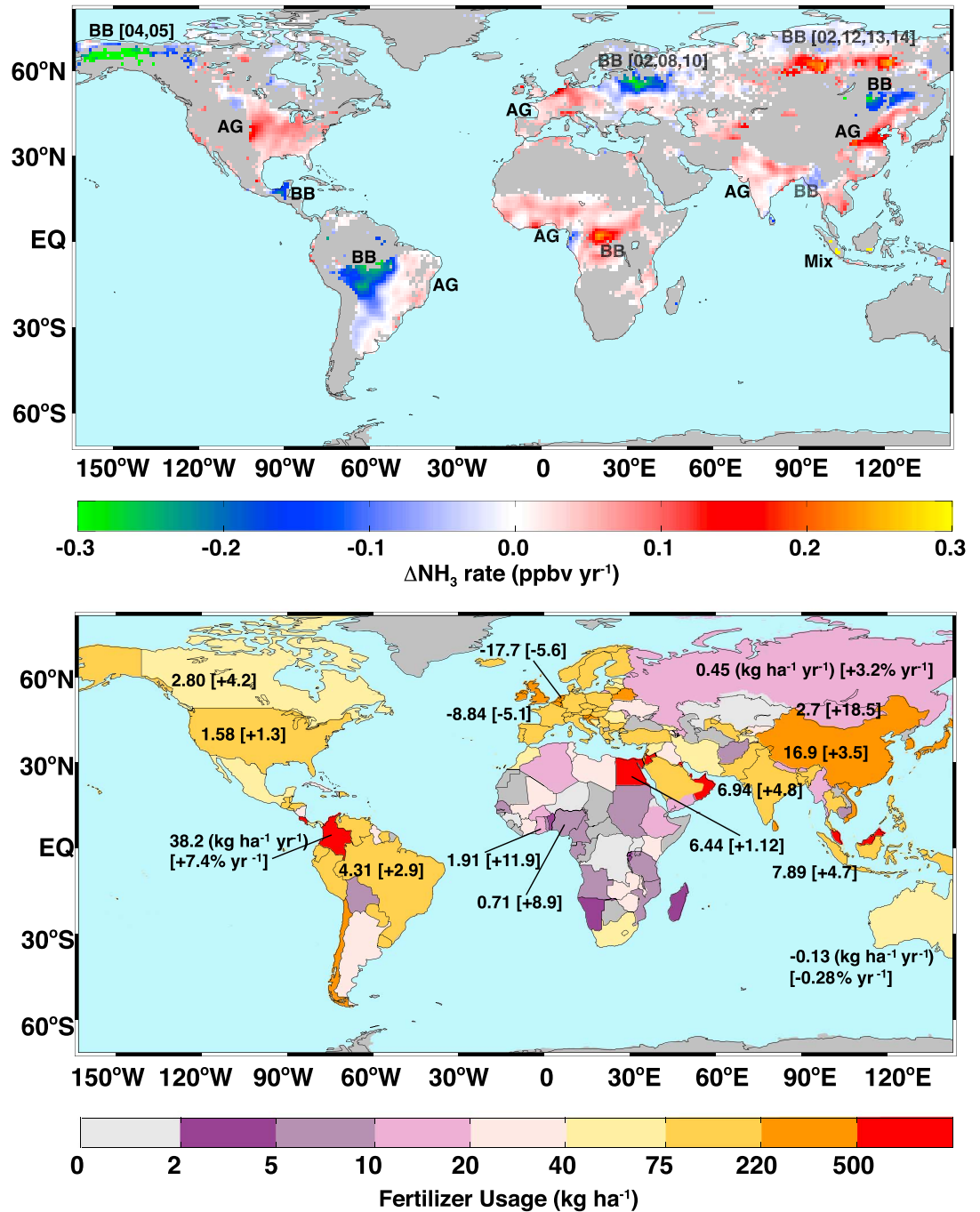


Figure 1. Trend in AIRS NH₃. (top) Temporal trends (+0.3 to −0.3 ppbv yr^{−1}). The locations and the last two digits of the years of biomass burning events (in square brackets) are marked as BB. The main agricultural regions are marked as AG. (bottom) National averaged annual N fertilizer usage in 2002–2013 in kg ha^{−1} and trends (percentage changes) in kg ha^{−1} yr^{−1} (% yr^{−1}); see text for details.

usage, trends between 2002 and 2013, and percentage trends) from the World Bank (<http://data.worldbank.org/indicator/AG.CON.FERT.ZS>) is plotted in Figure 1 (bottom).

AIRS reveals both increases and decreases over disparate parts of the globe. Biomass burning related decreases are seen over Alaska, the central district of Russia and eastern Europe, Mongolia, inner Mongolia, NE China, the Yucatan of Mexico, and the Amazon in western Brazil; increases are seen over Siberia and Indonesia. These large fire events are highly episodic, often driven by one or two outlier years

(see Figure 1, top) and are not statistically robust. We focus on regions where such events have minimal influence. Significant NH_3 increases are seen over the American Midwest and Southern California (U.S.); east central China; the European Union (EU) countries (e.g., the Netherlands, Germany, Denmark, and Po Valley, Italy); parts of South Asia (i.e., Bangladesh, India, Pakistan, Cambodia, and Vietnam), South America (Brazil, Colombia, Ecuador, and parts of Peru), central Africa (Nigeria, Ghana, Sierra Leone, and Guinea), the Nile Delta of Egypt, and Fergana Valley, Uzbekistan. Regions with increasing trends are generally associated with anthropogenic emissions due to intense agricultural (e.g., related to NH_3 emissions) and changing acid precursor (SO_2 and NO_x) emissions.

Parts of Brazil and parts of Africa have seen substantial increases in ammonia concentrations, but trends in the tropics are complicated by their proximity to major areas of biomass burning, a highly variable source of NH_3 . Fertilizer use increase in 2002–2013, e.g., $4.3 \text{ kg ha}^{-1} \text{ yr}^{-1}$ ($+2.9\% \text{ yr}^{-1}$) over Brazil and $0.71 \text{ kg ha}^{-1} \text{ yr}^{-1}$ ($+8.9\% \text{ yr}^{-1}$) over Nigeria (see Figure 1, bottom), can largely explain the NH_3 increase over these regions.

4. Regional Ammonia Trends and Their Driving Mechanisms

Figure 2 (left column) shows 14 year mean NH_3 VMRs for four regions with intense agricultural activities, the U.S., China, the EU, and South Asia, where the blue boxes in each panel outline the areas used in the trend computations. The underlying maps were selected using previously defined frequent occurrences of elevated NH_3 concentrations and good measurement sensitivities of AIRS [Warner *et al.*, 2016]. Highest concentrations were observed over densely populated and heavily farmed South Asia followed by northeast China where a high percentage of land is used for fertilized crops [Huang *et al.*, 2012].

AIRS trend analysis (Figure 3) shows that NH_3 concentrations have increased over the U.S. by $0.056 \pm 0.011 \text{ ppbv yr}^{-1}$ ($\sim 2.61\% \text{ yr}^{-1}$), over China by $0.076 \pm 0.020 \text{ ppbv yr}^{-1}$ ($\sim 2.27\% \text{ yr}^{-1}$), and the EU by $0.053 \pm 0.021 \text{ ppbv yr}^{-1}$ ($\sim 1.83\% \text{ yr}^{-1}$); error bars represent $\pm 1\sigma$ standard deviations and the percent increase is based on the mean concentration. The increasing trends in Figure 3 are significant at the 95% confidence level for NH_3 over the American Midwest, the EU, and China with p values at 0.0003, 0.026, and 0.0028, respectively. South Asia shows only a slight increase ($0.0098 \pm 0.019 \text{ ppbv yr}^{-1}$) that is not statistically significant (p value = 0.61). In Figure 3, the monthly mean AIRS NH_3 VMRs at 918 hPa are plotted from September 2002 to August 2016 with proper quality assurance and screening by frequent occurrences. The trends, however, were linearly fitted using the yearly averaged values.

Over the U.S., the Midwest shows significant increases in NH_3 , but fertilizer use has grown only modestly ($\sim 1.3\% \text{ yr}^{-1}$) and total food consumption has remained constant within observational uncertainty. Additionally, wet deposition of NH_4^+ does not show any discernable trend [Lajtha and Jones, 2013].

What then is the cause of the definitive growth in the concentration of NH_3 ? Increases can be attributed to a larger fraction remaining in the gas phase due to decreased removal to the condensed phase. For the period of 2003 to 2014 (latest year for which data are available) the U.S. Environmental Protection Agency reports an average NO_2 emissions decreasing at an average of $5.3\% \text{ yr}^{-1}$ and SO_2 decreasing at $9.0\% \text{ yr}^{-1}$ (<https://www.epa.gov/air-emissions-inventories/air-pollutant-emissions-trends-data>). Measurements from the Interagency Monitoring of Protected Visual Environments network indicate that U.S. annual mean ambient SO_2 and SO_4^{2-} concentrations have demonstrated consistent decreases [Hand *et al.*, 2012]. Satellite measurements from the Ozone Monitoring Instrument (OMI) [Krotkov *et al.*, 2016] of tropospheric NO_2 indicated a steady decrease ($-1.54\% \text{ yr}^{-1}$; p value = 0.003) from 2004 to 2016 (Figure 3, top). Emissions of SO_2 and NO_x from the electric power sector in 2012 declined to their lowest level since the passage of the Clean Air Act Amendments of 1990. The sum of emission level of SO_2 and NO_x in 2012 is approximately half of those in 2005 when Clean Air Interstate Rule, a cap-and-trade program intended to reduce SO_2 and NO_x beyond the levels defined by the acid rain program in the eastern half of the U.S., was announced. The decline in emissions is due primarily to an increasing number of coal-fired units retrofitted with scrubbers, to coal plants switching to lower sulfur coal, and low NO_x burners to limit NO_x emissions. Much of the increase in NH_3 over the U.S., especially after 2011, is thus an unintended consequence of successful measures to control acid deposition.

Year-to-year NH_3 variations over the U.S. are also affected by meteorological conditions. The highest NH_3 concentrations occurred in 2012 when the surface skin temperature anomaly was up to 4°K in the spring

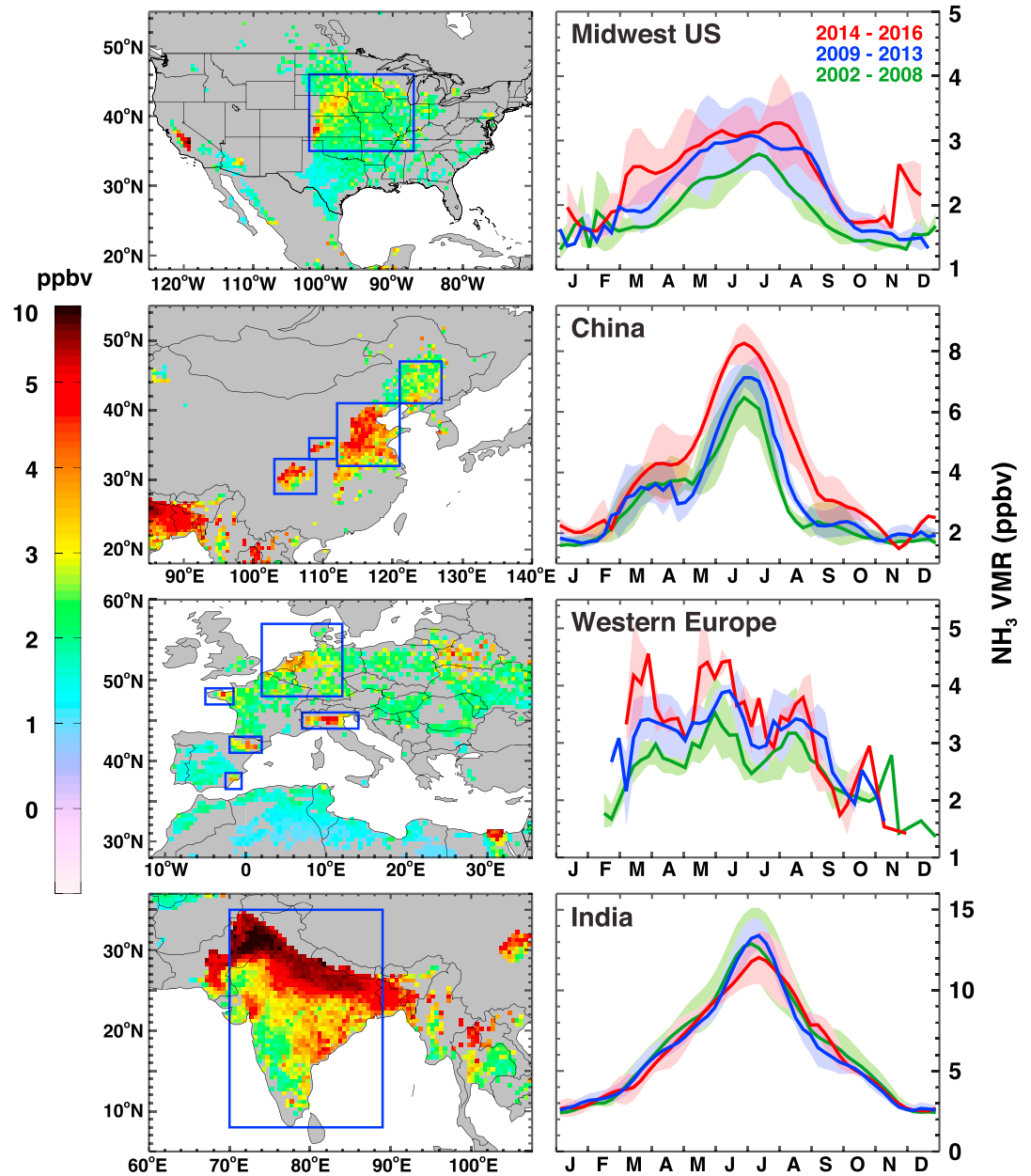


Figure 2. (left column) Regions with intense agricultural activities. The averaged 14 year NH_3 VMRs are shown for the (left column, first panel) American Midwest, (left column, second panel) China, (left column, third panel) EU, and (left column, fourth panel) South Asia. The blue boxes outline areas used in the trend studies. (right column) The seasonal variability in (right column, first panel) Midwest U.S., (right column, second panel) China, (right column, third panel) EU, and (right column, fourth panel) South Asia. The 7 day means of NH_3 VMRs at 918 hPa are averaged in 2002–2008 (green color), 2009–2013 (blue color), and 2014–2016 (red color) temporal bands, where broad solid lines represent the averages and shaded areas are within 1 sigma standard deviations.

and summer months and the total precipitation anomaly was the lowest in the 14 year history (Figure 3; negative 3 cm; shaded areas). Increased skin temperatures facilitate higher NH_3 emission rates, and decreased precipitation reduces scavenging of NH_3 gas, although a minimal level of soil moisture is necessary for NH_3 release. Hot, dry summers were conducive to high NH_3 concentrations in 2012 and 2006. From September 2002 to August 2016, the average surface skin temperatures in the U.S. Midwest increased by an average of $0.056^\circ\text{Kyr}^{-1}$ using March–August data. Using the published ammonia temperature dependence (see section 2.2), we can approximate the contribution from increasing

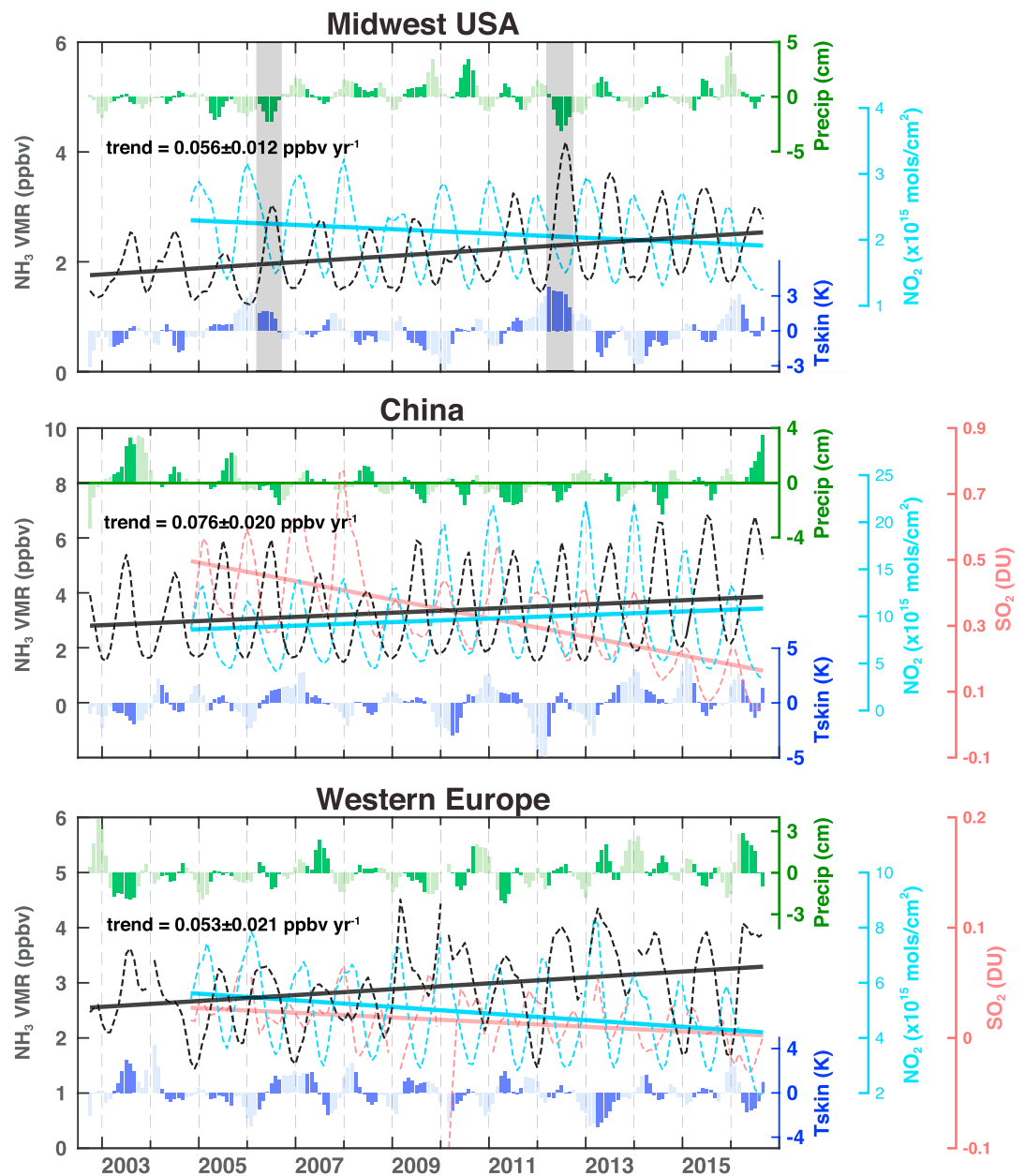


Figure 3. The recent (~14 year) trends of AIRS NH₃ concentrations. The NH₃ concentrations (i.e., VMRs in ppbv) at 918 hPa are shown in black dashed curves, with linear fits in solid lines, for (top) Midwest U.S., (middle) China, and (bottom) EU averaged in each region, respectively. The NH₃ increasing trends are correlated with OMI SO₂ decreasing trends (red color curve; shown only for China and EU) and NO₂ trends (cyan color). Also shown are the surface skin temperature anomaly (K; in blue color bars) and total precipitation anomaly (cm; in green color bars) from the ECMWF ERA-Interim reanalysis.

temperatures during this period as $0.65\% \text{ yr}^{-1}$ or approximately 25% of the total ($2.61\% \text{ yr}^{-1}$) increase observed. Note that these temperature trends are highly uncertain considering the fitting is not significant (p value = 0.19). The effects of variability in climate, which strongly influence NH₃ emission, also influence deposition of NH₃ and the partitioning between gas and aerosol phase [Fowler *et al.*, 2015]. Higher air temperatures will reduce the stability of ammonium nitrate aerosols, leading to higher VMRs of NH₃.

The seasonal cycle for the U.S. (Figure 2, first row) shows a broad peak from April to September corresponding to growing season and warmest temperatures; most of the increase is seen in these months. This figure also shows a recent broadening of the maximum, possibly related to warmer temperatures in spring and fall.

Over the EU region, increased NH_3 concentrations appear to be due almost entirely to the decline of SO_2 ($-0.0021 \pm 0.0007 \text{ DU yr}^{-1}$ and $-14.12\% \text{ yr}^{-1}$) and NO_2 ($-0.12 \pm 0.0196 \times 10^{15} \text{ molecules/cm}^2 \text{ yr}^{-1}$ and $-2.44\% \text{ yr}^{-1}$), according to OMI observations (Figure 3, bottom); aerosol loading over Europe has likewise declined between 1998 and 2010 [Hsu *et al.*, 2012]. A number of regulations on air quality protection existed in EU since 1980, yet a Directive of the European Parliament and of the Council on ambient air quality and cleaner air for Europe was established in 2008 as a basic legal instrument regulating air quality management [Kuklinska *et al.*, 2015]. This new directive obligates the EU members to implement plans to meet the permissible levels of certain substances. Possibly due to this action, as well as the economic crisis, the OMI SO_2 showed a sudden reduction and AIRS NH_3 showed a sudden increase in 2009 and remained at nearly the same level. The relatively small NH_3 increase compared to other major agricultural regions may be partially due to decreases in nitrogenous fertilizer use, e.g., $-5.2 \text{ kg ha}^{-1} \text{ yr}^{-1}$ ($-0.3\% \text{ yr}^{-1}$) from the World Bank 2016 database and U.S. Department of Agriculture, World Fertilizer Consumption Statistics, and International Fertilizer Industry Association, Paris, 2015 (<http://www.fertilizer.org/Statistics>). Concentrated animal feeding operations are another major contributor to NH_3 emissions and have increased in the EU countries (e.g., Food and Agriculture Organization of the United Nations; <http://faostat.fao.org>) and in the U.S. (<http://www.factoryfarmmap.org/-animal:cattle;location:US;year:2012>). The surface skin temperature influence on the NH_3 trends in the EU regions was not studied, due to low-temperature trends and lack of significance (e.g., $-0.0125^\circ\text{K yr}^{-1}$ with p value = 0.70). The seasonal cycle over the EU (Figure 2, right column, third panel) is modest, reflecting the weak seasonality in temperature and precipitation.

Over China, the increasing trend of NH_3 ($0.076 \text{ ppbv yr}^{-1}$) appears to be related to decreased sulfur emissions, increased fertilizer use, and increasing local temperatures. The OMI SO_2 indicate an irregular but discernable decreasing trend (Figure 3) while fertilizer application has increased at a rate of $3.5\% \text{ yr}^{-1}$ over roughly the time period of our AIRS measurements, according to the World Bank (<http://data.worldbank.org/indicator/AG.CON.FERT.ZS>). Decreases in OMI SO_2 ($-0.028 \pm 0.0052 \text{ DU yr}^{-1}$ or $-8.48\% \text{ yr}^{-1}$) (Figure 3, middle) generally track NH_3 increases. An exception to the anticorrelation between SO_2 and NH_3 is the reduction of both species in 2008 driven by aggressive pollution reduction measures associated with the Beijing Olympic Games [Wang *et al.*, 2009]. Chinese pollution control legislations are in 5 year increments, with the eleventh 5 year plan (FYP) in 2005–2010 aiming to reduce SO_2 , while the twelfth between 2011 and 2015 aiming to reduce SO_2 and NO_x (<http://wenku.baidu.com/link?url=LdcQKxikl-HYhK7uONVne4e5-ikl5Ukvg3iMVMX37E4LLbIYYfR0s0kdRUBwxydVmZYUcVCFbKyytqxxJPG4kbMQqiUyVahVdc95ZKTiG>). The significant SO_2 emission drop in northeastern China in 2008 and later are because the eleventh FYP mandates the installation of emission control devices for power and steel plants. The NH_3 concentrations increased in 2009 and stayed consistently higher than before 2009 period (see Figure 2, right column, second panel), correlating well with the SO_2 reduction. The OMI NO_2 shows increases over China through 2014, then a fast decreasing in 2015 and 2016 at the end of the twelfth FYP. The NH_3 concentration has reached the highest values in China in 2014–2016 in response to the lowest SO_2 and NO_2 values in our data records. Studies of the response of ammonia emissions to temperature have been conducted primarily in North America and Europe, making extrapolation to Asian soils more uncertain, but if we apply these factors to China, increases in surface skin temperature of $0.0969^\circ\text{K yr}^{-1}$ (p value = 0.0057) in spring and summer explain an increase of approximately $1.12\% \text{ yr}^{-1} \text{ NH}_3$.

The seasonal cycle over China (Figure 2, right column, second panel) shows a sharp peak in June and July corresponding to the warmest temperatures and local precipitation maximum. The monsoons generate a strong seasonal cycle in precipitation not seen over the U.S. or EU. A secondary maximum in spring corresponds to peak fertilizer application. The growing season has broadened over China during the period of study, as was observed for the U.S.

South Asia (Figure 2) shows the highest concentrations and strongest seasonal cycle but no significant trend over the past 14 years. Heavy fertilizer use and the highest reported number of cattle of any country lead to strong emissions in the warmer months. South Asia has a distinctive monsoon with ~80% of the precipitation falling in between June and September in Delhi. While winters are warm relative to the U.S., EU, and China, lack of soil moisture inhibits NH_3 production and release. Fertilizer use in South Asia has increased by $6.9 \text{ kg ha}^{-1} \text{ yr}^{-1}$ ($+4.8\% \text{ yr}^{-1}$) from 2002 to 2013, according to the World Bank. The surface skin temperature influence on the NH_3 trends in South Asia is not studied, due to missing data arising from the uncertainties in

summer monsoons and the small NH_3 trends. Increased emissions are not reflected in the AIRS observations because recent increases in SO_2 , $3.25\% \text{ yr}^{-1}$ (p value = 0.047), and NO_x , $1.22\% \text{ yr}^{-1}$ (p value = 0.0002), from uncontrolled coal combustion and other sources have led to greater conversion of gaseous NH_3 into particulate sulfates and nitrates. Monitoring with sun photometers indicates a substantial increase in aerosol concentrations over recent years [Hsu et al., 2012].

5. Conclusions

The 14 year AIRS satellite record indicates substantial, statistically significant increases in ammonia over several of the world's major agricultural regions, with deleterious effects on vegetation and ecosystem health. Over the U.S., increases in NH_3 appear to be due to control of SO_2 and NO_x (an unintended consequence of successful acid rain regulations) and due to regionally warming temperatures. Over the EU, NH_3 concentrations have increased despite reduced fertilizer use, again due to improved control of sulfur and nitrogen oxide emissions. Over China, a combination of expanded agricultural activities, nascent SO_2 control measures, and increasing temperatures cause the observed increases in ammonia. Over South Asia, increased NH_3 emissions from growing fertilizer use are likely masked by simultaneous increases in SO_2 and NO_x emissions, resulting in increased concentrations of fine aerosols with adverse health effects.

The observed trends deduced here can guide numerical simulation of tropospheric ammonia and inform policy to mitigate disruption of biogeochemical nitrogen cycles and improve air quality. Complete validation of this satellite ammonia product is needed using long-term ground, as well as new airborne measurements as they become available. Ammonia trend monitoring efforts will continue through the lifetime of AIRS sensor and with current and future operational sensors such as IASI and Cross-track Infrared Sounder preferably using consistent algorithms.

Acknowledgments

This study was funded by NASA's The Science of Terra and Aqua program under grant numbers NNX11AG39G and NNX12AJ05G. We wish to acknowledge the AIRS, OMI, GEOS-Chem, and ECMWF science teams. R.R.D. was a member of AQUEST. MERRA data used in this study/project have been provided by GMAO at NASA Goddard Space Flight Center through the NASA GES DISC online archive. Computations were performed on the NASA Center for Climate Simulation (NCCS) super computing system. The observational data that support the findings of this study are available on the website via the corresponding author (J.X.W.) (http://atmos.umd.edu/~juying/GRL_2017_AIRS_NH3).

References

- Abbatt, J. P. D., S. Benz, D. J. Cziczko, Z. Kanji, U. Lohmann, and O. Mohler (2006), Solid ammonium sulphate aerosols as ice nuclei: A pathway for cirrus cloud formation, *Science*, *313*, 1770, doi:10.1126/science.1129726.
- Adams, P. J., J. H. Seinfeld, D. Koch, L. Mickley, and D. Jacob (2001), General circulation model assessment of direct radiative forcing by the sulfate–nitrate–ammonium–water inorganic aerosol system, *J. Geophys. Res.*, *106*, 1097–1111, doi:10.1029/2000JD900512.
- Barnes, I., and K. J. Rudzinski (Eds.) (2006), *Environmental Simulation Chambers: Application to Atmospheric Chemical Processes*, 458 pp., Springer, Netherlands.
- Beer, R., et al. (2008), First satellite observations of lower tropospheric ammonia and methanol, *Geophys. Res. Lett.*, *35*, L09801, doi:10.1029/2008GL033642.
- Berrisford, P., D. Dee, P. Poli, R. Brugge, K. Fielding, M. Fuentes, P. Kallberg, S. Kobayashi, S. Uppala, and A. Simmons (2011), The ERA-Interim archive version 2.0, *ERA Report Series 1, ECMWF*, Shinfield Park, Reading, U. K.
- Clarisse, L., C. Clerbaux, F. Dentener, D. Hurtmans, and P.-F. Coheur (2009), Global ammonia distribution derived from infrared satellite observations, *Nat. Geosci.*, *2*(7), 479–483, doi:10.1038/ngeo551.
- Dee, D. P., et al. (2011), The ERA-Interim reanalysis: Configuration and performance of the data assimilation system, *Q. J. R. Meteorol. Soc.*, *137*, 553–597, doi:10.1002/qj.828.
- Deeter, M. N., D. P. Edwards, J. C. Gille, and J. R. Drummond (2007), Sensitivity of MOPITT observations to carbon monoxide in the lower troposphere, *J. Geophys. Res.*, *112*, D24306, doi:10.1029/2007JD008929.
- Dentener, F. J., and P. J. Crutzen (1994), A three-dimensional model of the global ammonia cycle, *J. Atmos. Chem.*, *19*, 331–369.
- Erisman, J. W., M. A. Sutton, J. Galloway, Z. Klimont, and W. Winiwarter (2008), How a century of ammonia synthesis changed the world, *Nat. Geosci.*, *1*(10), 636–639, doi:10.1038/ngeo325.
- Erisman, J. W., J. N. Galloway, S. Seitzinger, A. Bleeker, N. B. Dise, R. Petrescu, A. M. Leach, and W. de Vries (2013), Consequences of human modification of the global nitrogen cycle, *Philos. Trans. R. Soc. B*, *368*, 1621, doi:10.1098/rstb.2013.0116.
- Fowler, D., et al. (2013), The global nitrogen cycle in the twenty-first century, *Philos. Trans. R. Soc. B*, *368*, 20130164, doi:10.1098/rstb.2013.0164.
- Fowler, D., et al. (2015), Effects of global change during the 21st century on the nitrogen cycle, *Atmos. Chem. Phys.*, *15*, 13,849–13,893, doi:10.5194/acp-15-13849-2015.
- Friedl, M. A., D. Sulla-Menashe, B. Tan, A. Schneider, N. Ramankutty, A. Sibley, and X. M. Huang (2010), MODIS collection 5 global land cover: Algorithm refinements and characterization of new datasets, *Remote Sens. Environ.*, *114*(1), 168–182, doi:10.1016/j.rse.2009.08.016.
- Galloway, J. N., and E. B. Cowling (2002), Reactive nitrogen and the world: 200 years of change, *Ambio*, *31*(2), 64–71, doi:10.1579/0044-7447-31.2.64.
- Galloway, J. N., et al. (2004), Nitrogen cycles: past, present, and future, *Biogeochemistry*, *70*(2), 153–226.
- Galloway, J. N., A. R. Townsend, J. W. Erisman, M. Bekunda, Z. Cai, J. R. Freney, L. A. Martinelli, S. P. Seitzinger, and M. A. Sutton (2008), Transformation of the nitrogen cycle: Recent trends, questions, and potential solutions, *Science*, *320*, 889–892.
- Garcia, D. (2010), Robust smoothing of gridded data in one and higher dimensions with missing values, *Comput. Stat. Data Anal.*, *54*, 1167–1178, doi:10.1016/j.csda.2009.09.020.
- Giglio, L., J. T. Randerson, G. R. Van der Werf, P. S. Kasibhatla, G. J. Collatz, D. C. Morton, and R. S. DeFries (2010), Assessing variability and long-term trends in burned area by merging multiple satellite fire products, *Biogeosciences*, *7*, 1171–1186, doi:10.5194/bg-7-1171-2010.
- Hand, J. L., B. A. Schichtel, W. C. Malm, and M. L. Pitchford (2012), Particulate sulfate ion concentration and SO_2 emission trends in the United States from the early 1990s through 2010, *Atmos. Chem. Phys.*, *12*, 10,353–10,365, doi:10.5194/acp-12-10353-2012.

- Hauglustaine, D. A., Y. Balkanski, and M. Schulz (2014), A global model simulation of present and future nitrate aerosols and their direct radiative forcing of climate, *Atmos. Chem. Phys.*, *14*, 11,031–11,063, doi:10.5194/acp-14-11031-2014.
- Henze, D. K., D. T. Shindell, F. Akhtar, R. J. D. Spurr, R. W. Pinder, D. Loughlin, M. Kopacz, K. Sing, and C. Shim (2012), Spatially refined aerosol direct radiative forcing efficiencies, *Environ. Sci. Technol.*, *46*, 9511–9518, doi:10.1021/es301993s.
- Hsu, N. C., R. Gautam, A. M. Sayer, C. Bettenhausen, C. Li, M. J. Jeong, S.-C. Tsay, and B. N. Holben (2012), Global and regional trends of aerosol optical depth over land and ocean using SeaWiFS measurements from 1997 to 2010, *Atmos. Chem. Phys.*, *12*(17), 8037–8053.
- Huang, X., Y. Song, M. Li, J. Li, Q. Huo, X. Cai, T. Zhu, M. Hu, and H. A. Zhang (2012), High-resolution ammonia emission inventory in China, *Global Biogeochem. Cycles*, *26*, GB1030, doi:10.1029/2011GB004161.
- Krotkov, N. A., et al. (2016), Aura OMI observations of regional SO₂ and NO₂ pollution changes from 2005 to 2015, *Atmos. Chem. Phys.*, *16*, 4605–4629, doi:10.5194/acp-16-4605-2016.
- Kuklinska, K., L. Wolska, and J. Namiesnik (2015), Air quality policy in the U.S. and the EU-A review, *Atmos. Pollut. Res.*, *6*, 129–137, doi:10.5094/APR.2015.015.
- Lajtha, K., and J. Jones (2013), Trends in cation, nitrogen, sulfate and hydrogen ion concentrations in precipitation in the United States and Europe from 1978 to 2010: A new look at an old problem, *Biogeochemistry*, *116*(1-3), 303–334.
- Lelieveld, J., J. S. Evans, M. Fnais, D. Giannadaki, and A. Pozzer (2015), The contribution of outdoor air pollution sources to premature mortality on a global scale, *Nature*, *525*(7569), 367–371.
- Malm, W. C., B. A. Schichtel, M. L. Pitchford, L. L. Ashbaugh, and R. A. Eldred (2004), Spatial and monthly trends in speciated fine particle concentration in the United States, *J. Geophys. Res.*, *109*, D03306, doi:10.1029/2003JD003739.
- Martin, S. T., H.-M. Hung, R. J. Park, D. J. Jacob, R. J. D. Spurr, K. V. Chance, and M. Chin (2004), Effects of the physical state of tropospheric ammonium-sulfate-nitrate particles on global aerosol direct radiative forcing, *Atmos. Chem. Phys.*, *4*, 183–214, doi:10.5194/acp-4-183-2004.
- Pope, C. A., R. T. Burnett, M. J. Thun, E. E. Calle, D. Krewski, K. Ito, and G. D. Thurston (2002), Lung cancer, cardiopulmonary, mortality, and long-term exposure to fine particulate air pollution, *J. Am. Med. Assoc.*, *287*, 1132–1141.
- Riddick, S., D. Ward, P. Hess, N. Mahowald, R. Massad, and E. Holland (2016), Estimate of changes in agricultural terrestrial nitrogen pathways and ammonia emissions from 1850 to present in the Community Earth System Model, *Biogeosciences*, *13*(11), 3397–3426.
- Schiferl, L. D., et al. (2016), Interannual variability of ammonia concentrations over the United States: Sources and implications, *Atmos. Chem. Phys.*, *16*, 12,305–12,328, doi:10.5194/acp-16-12305-2016.
- Sheppard, L. J., I. D. Leith, T. Mizunuma, J. N. Cape, A. Crossley, S. Leeson, M. A. Sutton, N. V. Dijk, and D. Fowler (2011), Dry deposition of ammonia gas drives species change faster than wet deposition of ammonium ions: Evidence from a long-term field manipulation, *Global Change Biol.*, *17*, 3589–3607, doi:10.1111/j.1365-2486.2011.02478.x.
- Streets, D. G., et al. (2003), An inventory of gaseous and primary aerosol emissions in Asia in the year 2000, *J. Geophys. Res.*, *108*(D21), 8809, doi:10.1029/2002JD003093.
- Sutton, M. A., et al. (2007), Challenges in quantifying biosphere-atmosphere exchange of nitrogen species, *Environ. Pollut.*, *150*, 125–139, doi:10.1016/j.envpol.2007.04.014.
- Sutton, M., J. Erisman, F. Dentener, and D. Moller (2008), Ammonia in the environment: From ancient times to the present, *Environ. Pollut.*, *156*, 583–604, doi:10.1016/j.envpol.2008.03.013.
- Van Damme, M., J. W. Erisman, L. Clarisse, E. Dammers, S. Whitburn, C. Clerbaux, A. J. Dolman, and P.-F. Coheur (2015), Worldwide spatio-temporal atmospheric ammonia (NH₃) columns variability revealed by satellite, *Geophys. Res. Lett.*, *42*, 8660–8668, doi:10.1002/2015GL065496.
- Wang, Y., J. Hao, M. B. McElroy, J. W. Munger, H. Ma, D. Chen, and C. P. Nielsen (2009), Ozone air quality during the 2008 Beijing Olympics: Effectiveness of emission restrictions, *Atmos. Chem. Phys.*, *9*(14), 5237–5251.
- Wang, Y., Q. Q. Zhang, K. He, Q. Zhang, and L. Chai (2013), Sulfate-nitrate-ammonium aerosols over China: Response to 2000–2015 emission changes of sulfur dioxide, nitrogen oxides, and ammonia, *Atmos. Chem. Phys.*, *13*, 2635–2652, doi:10.5194/acp-13-2635-2013.
- Warner, J. X., Z. Wei, L. L. Strow, R. R. Dickerson, and R. Nowak (2016), Global ammonia sources seen by AIRS 13-years measurements, *Atmos. Chem. Phys.*, *16*, 5467–5479, doi:10.5194/acp-16-5467-2016.